ChemSusChem

Research Article
doi.org/10.1002/cssc.202200614

**Chemistry
Europe**
European Chemical
Societies Publishing

www.chemsuschem.org

A Survey of Catalytic Materials for Ammonia Electrooxidation to Nitrite and Nitrate

Sam Johnston,[a] Sam Cohen,[a, b] Cuong K. Nguyen,[a] Khang N. Dinh,[a] Tam D. Nguyen,[a]
Sarbjit Giddey,[b] Christopher Munnings,[b] Alexandr N. Simonov,*[a] and
Douglas R. MacFarlane*[a]

Studies of the ammonia oxidation reaction (AOR) for the synthesis of nitrite and nitrate ($NO_{2/3}^-$) have been limited to a small number of catalytic materials, majorly Pt based. As the demand for nitrate-based products such as fertilisers continues to grow, exploration of alternative catalysts is needed. Herein, 19 metals immobilised as particles on carbon fibre electrodes were tested for their catalytic activity for the ammonia electrooxidation to $NO_{2/3}^-$ under alkaline conditions (0.1 м KOH). Nickel-based electrodes showed the highest overall $NO_{2/3}^-$ yield with a rate of 5.0 ± 1.0 nmol s^{-1} cm^{-2}, to which nitrate contributed $62 \pm 8\%$. Cu was the only catalyst that enabled formation of nitrate, at a rate of 1.0 ± 0.4 nmol s^{-1} cm^{-2}, with undetectable amounts of nitrite produced. Previously unexplored in this

context, Fe and Ag also showed promise and provided new insights into the mechanisms of the process. Ag-based electrodes showed strong indications of activity towards NH_3 oxidation in electrochemical measurements but produced relatively low $NO_{2/3}^-$ yields, suggesting the formation of alternate oxidation products. $NO_{2/3}^-$ production over Fe-based electrodes required the presence of dissolved O_2 and was more efficient than with Ni on longer timescales. These results highlight the complexity of the AOR mechanism and provide a broad set of catalytic activity and nitrate versus nitrite yield data, which might guide future development of a practical process for the distributed sustainable production of nitrates and nitrites at low and medium scales.

Introduction

Electrochemical oxidation of ammonia has been widely studied for over a century. With studies dating back as far as 1904,[1] the ammonia oxidation reaction (AOR) has been researched in the context of chemical sensors,[2–4] remediation of ammonia containing wastewater systems,[5–9] liberation of stored hydrogen where ammonia is the hydrogen carrier,[10,11] and for fuel cell applications.[12–15] Studies spanning from the early 1950s to 1970[16–19] were the first examples of detailed mechanistic investigations into the AOR, with the landmark paper by Gerischer and Mauerer (1970) proposing what is now the most widely accepted model of the electrochemical ammonia oxidation on platinum.[19] These early studies served to form the basis for the majority of research that followed.[20]

[a] Dr. S. Johnston, S. Cohen, Dr. C. K. Nguyen, Dr. K. N. Dinh, Dr. T. D. Nguyen,
Dr. A. N. Simonov, Prof. D. R. MacFarlane
School of Chemistry
Monash University
Clayton, VIC 3800 (Australia)
E-mail: alexandr.simonov@monash.edu
douglas.macfarlane@monash.edu
[b] S. Cohen, Dr. S. Giddey, Dr. C. Munnings
CSIRO Energy
Private Bag 10, Clayton South, Victoria 3169 (Australia)

At present, the bulk of studies of the ammonia electrooxidation have focused on a few key materials. Most of the pioneering research was conducted on platinum,[17–19] and due to its proven activity a robust body of literature has formed around it.[21,22] However, platinum-based AOR catalysts suffer from some common issues, the most pervasive of which is their tendency to become rapidly poisoned during operation.[19,21]

In more recent times, studies have expanded into the use of non-platinum based metals as ammonia oxidation catalysts.[20] Nickel has emerged as a prime candidate, with a number of reports suggesting it to be active for ammonia oxidation to N_2.[23–25] In addition to nickel-based catalysts, gold, silver, copper,[26] and anodised aluminium[24] have also been investigated, but with limited positive results. However, as with most other literature in this field, these studies are limited by their intended application. As the bulk of the research conducted has been primarily focused on applications where the desired ammonia oxidation product is dinitrogen, other potentially useful products, such as NO_2^- and NO_3^- (henceforth referred to collectively as $NO_{2/3}^-$), have gone largely ignored. In the context of a fuel cell or bioremediation project this is completely understandable as the production of $NO_{2/3}^-$ is clearly undesirable. As such, $NO_{2/3}^-$ formation is often not tested for or is simply not classified as a valid form of activity. However, $NO_{2/3}^-$ are not intrinsically without value. The immense field of agriculture for example, is largely reliant on the anthropogenic production of NO_3^- from ammonia for use as fertiliser compounds.[27]

Currently, the primary large scale method for converting NH_3 into N-based fertilisers such as nitrates is via the Ostwald process.[28,29] In this process, ammonia is converted into a

ChemSusChem

Research Article
doi.org/10.1002/cssc.202200614

Chemistry
Europe
European Chemical
Societies Publishing

solution of nitric acid in a multistage chemical reaction catalysed by a Pt/Rh gauze. The nitric acid generated then serves as the feedstock for conversion into the desired product, for example ammonium or potassium nitrate. While the Ostwald process is reliable and relatively energy efficient, the initial oxidation reaction suffers from a 2 to 7% loss, where ammonia is converted into nitrous oxide (N_2O) or dinitrogen gas via the side-reactions 1 and 2.[28]

$$2NH_{3(g)} + 2O_2 \rightleftharpoons N_2O + 3H_2O_{(g)} \qquad (1)$$

$$2NH_{3(g)} + 3/2O_2 \rightleftharpoons N_2 + 3H_2O_{(g)} \qquad (2)$$
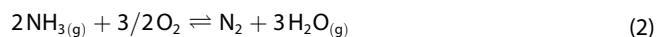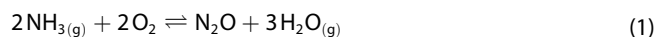
Due to the large production scale of nitrogenous products and the fact that N_2O is a highly potent greenhouse gas (global warming potential 298 times that of CO_2),[30] this seemingly small loss is significant. While there have been several mitigation techniques developed to deal with these emissions, they all come at a considerable cost.[28]

As with nitrate, nitrite is used in a variety of industrial scale applications. While it is commonly known that nitrite is used as a curing agent for meat products due to its antimicrobial properties[31] it is perhaps less known that nitrite is a key feedstock compound in the chemical and pharmaceutical industries. Nitrite is used as a reagent in the production of a wide variety of products from synthetic caffeine to the production of herbicides such as Pyramin® and many other nitroso and isonitroso compounds.[31] Nitrite has also found use as an anti-corrosion agent for the treatment of metal surfaces such as carbon steel.[32]

The production of nitrite on an industrial scale is a variant of the Ostwald process wherein the NO and NO_2 intermediates are passed through a solution of sodium carbonate and sodium hydroxide to generate sodium nitrite and carbon dioxide (reaction 3).[31]

$$NO + NO_2 + 2NaOH + Na_2CO_3 \rightleftharpoons 2NaNO_2 + CO_2 + H_2O \qquad (3)$$
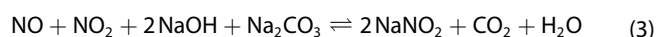
As the basis of the production of nitrite is essentially identical to that of nitrate, it shares the shortcomings of the NO_3^- production with the added implication of 1 CO_2 molecule produced for every 2 NO_2^- anions generated.

When the issues discussed above are considered, the electrochemical conversion of ammonia to $NO_{2/3}^-$ becomes an attractive alternative. Development of a system focused on the exclusive generation of NO_2^- could lead to the development of online nitrite production systems to feed large scale chemical reactions. On the other hand, the development of a robust electrochemical AOR system coupled to a suitable oxygen reduction cathode for the exclusive generation of NO_3^- would enable the construction of small scale, distributed fertiliser plants powered by renewable energy sources.

Several groups have reported the formation of $NO_{2/3}^-$ as side-products during the NH_3 electrooxidation to N_2. For example, Almomani et al. found that nickel oxide nanoparticles catalyse electrooxidation of ammonia to N_2 as the primary oxidation product in a solution of 0.1 M $NaNO_3$ + 0.2 M NH_4OH

(pH 9) at a constant current density of 30 mA cm^{-2} but with small amounts of nitrite and nitrate generated.[33] Tsai et al. explored the use of CuCo/Ni-foam electrodes for the electro-oxidation of ammonia at 1.1 V vs. Ag│AgCl (unspecified Cl$^-$ concentration) for wastewater remediation (using 10 mM $NaSO_4$ adjusted to pH 11 and ~3 mM NH_3 as a model electrolyte solution) and observed an increase in the NO_3^- and NO_2^- concentrations from 0 to ca. 0.65 and 0.01 mM over a period of 4 h, respectively.[34]

A study carried out by Xu et al. compared the performance of ammonia oxidation to N_2 of electrodes modified with $Ni(OH)_2$ and $Ni_{0.8}Cu_{0.2}$ layered hydroxides under alkaline conditions (0.1 M NaOH).[35] During 24 h chronoamperometric measurements, 84% (1.26 mmol) of the initial 1.5 mmol of NH_3 added was oxidised when the NiCu-based electrode was employed. Of this, approximately 28% of the total product (0.35 mmol) was NO_3^-. In contrast, $Ni(OH)_2$ catalyst allowed for only 58% (0.87 mmol) of the initial ammonia concentration to be oxidised over the same period of time, but with a higher relative amount of NO_3^- produced (ca. 39%; 0.26 mmol).

Recognising the importance of the development of sustainable technologies for the production of nitrite/nitrate, some of the most recent investigations have focused on the conversion of ammonia to $NO_{2/3}^-$. One study conducted by the authors of the present work investigated the activity of copper metal electrodes for the AOR and identified two distinct catalytic mechanisms, the interplay of which defined the rate and products of the process. Specifically, homogeneous catalysis of NH_3 electrooxidation by dissolved $Cu^{2+/3+}$-based species, preferentially producing NO_2^- with up to 87% faradaic efficiency, was favoured at high pH (1.1 M KOH), while a heterogenous catalytic reaction was more prominent at lower KOH concentration (0.011 M) and positive potentials resulting in the predominant formation of NO_3^-.[36] The most recent study by Medvedev et al. explored the use of high surface area $Ni(OH)_2$ in phosphate and sulphate solutions to convert ammonia into nitrite/nitrate.[37] It was found that up to 72% faradaic efficiency for $NO_{2/3}^-$ and close to 100% conversion of ammonia is possible under these conditions.[37]

Thus, currently known AOR catalysts targeted at the generation of $NO_{2/3}^-$ are majorly limited to nickel, copper and combinations thereof. With the aim of supporting further development of efficient catalytic systems for this important process, we have undertaken a survey of nineteen commonly available metals to determine which of them exhibit meaningful activity towards the electrochemical conversion of ammonia to $NO_{2/3}^-$. In doing so, we demonstrate that both silver and iron, which were previously unrecognised in this context, are catalytically active for the AOR.

Results and Discussion

Aiming to compare the intrinsic electrocatalytic activity of different metals for the ammonia electrooxidation to nitrite and nitrate rather than achieve peak performance, we used relatively low material loadings of ca. 0.1 µmol cm^{-2} (per geo-

metric area of electrode surface). Such low amounts of the active materials precluded detection of the metal-based materials by X-ray diffraction analysis (Section 1 of the Supporting Information). Hence, X-ray photoelectron spectroscopy (XPS) was used to confirm the deposition of the desired materials on as-prepared electrodes (Section 2 of the Supporting Information). Scanning electron microscopy (SEM) was used to probe the morphology and particle size distribution of the best-performing catalysts on the carbon fibre surface (Section 3 of the Supporting Information). Most importantly, redox transformations of the metals were detected for all materials examined by cyclic voltammetry, confirming their successful deposition on the electrode surface in an electrochemically active state (Section 4 of the Supporting Information).

Although the electrodes were functionalised with metal precursors under reductive conditions (see Experimental Section for details), the very positive potentials required to achieve measurable rates of ammonia electrooxidation inevitably resulted in transformation, at least partially, of the tested materials into corresponding (hydr)oxides/oxyhydroxides. However, in the light of uncertainties in the compositions of the latter, all materials investigated herein are referred to below as the corresponding metal element, but we stress that this does not reflect the actual catalytic species. We also note that no special measures were taken to remove Fe contamination from the KOH electrolyte, meaning that all catalysts examined most likely contained small amounts of iron (hydr)oxide/oxyhydroxide species.[38,39]

All electrochemical measurements carried out in this work were conducted in two-compartment cells with low-porosity separators to avoid losses of the $NO_{2/3}^-$ products through electroreduction at the auxiliary electrode.

Material survey

During the initial stages of this work, each catalyst was assessed relative to its counterparts as having "low", "medium" or "high" activity for ammonia electrooxidation to nitrite and nitrate. Catalysts were judged based on three types of measurements: cyclic voltammetry, chronoamperometry and ion chromatographic analysis of nitrite and nitrate. It should be noted that, in the case of voltammetric and potentiostatic measurements, assigned classifications are not direct confirmation of the AOR to $NO_{2/3}^-$ activity but rather indicate that particular features or behaviours present in each measurement may indicate a certain degree of performance in this regard.

Comparative voltammetric measurements were conducted in 0.1 M KOH electrolyte solutions with and without 0.1 M NH_3 added. Determination of the degree of the AOR activity was made qualitatively based on the changes that occurred in voltammograms when ammonia was added to the solution relative to the measurement conducted in its absence. The addition of aqueous ammonia to an electrolyte solution can cause significant changes to existing peaks due to adsorption and redox reactions with the electrochemically generated surface species. However, not all changes are indicative of

activity towards the AOR.[40] Features considered to be valid signs of the catalytic activity were the appearance of new oxidative peaks, the enhancement or alteration of existing oxidation peaks and/or the appearance or alteration of reductive peaks. Both positive and negative shifts in the oxidative wave with respect to the signal from the competing oxygen evolution reaction (OER) measured in pure 0.1 M KOH were considered to be valid signs of activity towards the AOR. As NH_3 electrooxidation is a sluggish reaction and can occur in a similar potential range to the OER, catalysts that are active for both reactions can demonstrate minimal changes in the oxidative current in the presence of NH_3. If the activity for the OER is higher than for the AOR, the addition of ammonia to the electrolyte solution can suppress measured oxidation currents, while an increase is expected for the systems that are potent catalysts for the NH_3 oxidation but not for the O_2 evolution reaction. Thus, any prominent changes in the voltammetric data were considered as an indication of a measurable degree of the catalytic activity towards ammonia oxidation and such materials were thus classified as having "high" activity (see Figure 1A for an example).

When changes in voltammetric behaviour were seen at a significantly lower magnitude, the material was classified as likely having a "medium" level of catalytic activity towards ammonia oxidation. In addition to this, the appearance of previously unseen reductive peaks was also considered to be a sign of moderate ammonia oxidation activity, as these peaks might be associated with the reduction of $NO_{2/3}^-$ formed at positive potentials.[36] An example of a voltammogram with a "medium" classification is shown in Figure 1B. Lastly, when minor or insignificant changes occurred after ammonia was added to the electrolyte solution (exemplified in Figure 1C), the material being tested was classified as likely having a "low" degree of the activity towards ammonia oxidation. For averaged voltammograms of all materials tested refer to Section 4 of the Supporting Information.

As with voltammetric measurements, chronoamperometry was conducted in a comparative manner in 0.1 M KOH electrolyte solutions in the presence and absence of 0.1 M NH_3. As mentioned in the introductory section, there are known issues with the long-term use of ammonia oxidation catalysts, namely the tendency for the electrodes to become poisoned with adsorbed nitrogen (N_{ads}) and/or saturation by $NO_{2/3}^-$ products.[21] As each poisoning process is typically quite rapid,[21] 10 min chronoamperometric measurements were deemed sufficient for their detection. All measurements were conducted at a relatively positive potential of 2.000 ± 0.003 V vs. RHE. This was done in an effort to avoid false negatives for any materials that have high onset potentials for the AOR. While choosing a strongly positive potential was likely to give rise to a significant amount of oxygen evolution, thus compromising the AOR faradaic efficiency of the materials tested, it also served to identify the highest possible number of active catalysts. As performance optimisation is outside the scope of this study, this approach was considered suitable.

In terms of classification, chronoamperograms where the addition of ammonia caused a major change in the sustained

ChemSusChem

Research Article
doi.org/10.1002/cssc.202200614

Chemistry Europe
European Chemical
Societies Publishing
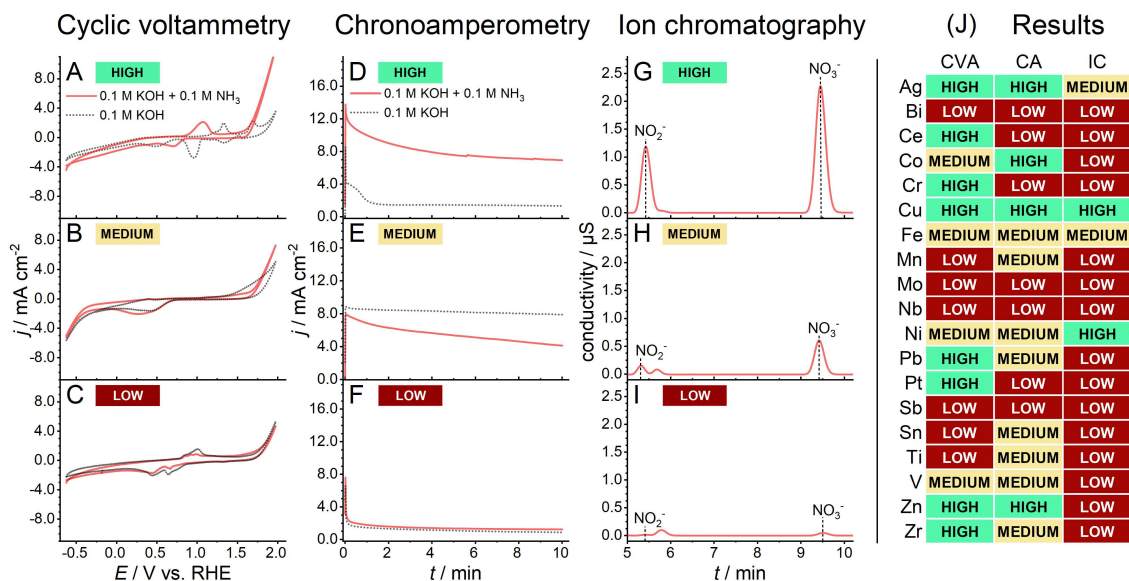
Figure 1. Examples of (A–C) cyclic voltammograms (scan rate, $v = 0.100\ V\,s^{-1}$), (D–F) chronoamperograms at 2.000 ± 0.003 V vs. RHE, and (G–F) ion chromatograms after the potentiostatic tests showing the examples of high (A, D, G), medium (B, E, H) and low (C, F, I) AOR activity criteria. (J) Tally of the results for the materials tested herein in each category. Electrochemical measurements were conducted in 0.1 M KOH electrolyte solutions without (dotted black) and with (solid red) 0.1 M NH_3 present; currents are normalised to the geometric surface area of the electrodes (1 cm^2).

current relative to the ammonia-free measurement were considered likely to have a high level of activity towards ammonia oxidation. As with changes in the oxidative wave in voltammetry, both increased and attenuated currents measured in the prescribed potentiostatic regime in the presence of ammonia were considered to be valid signs of activity (e.g., Figure 1D). Measurements where the difference in current was small or where there were signs of degrading current were classed as "medium" (e.g., Figure 1E).

For situations where the change in the chronoamperometric response in the presence of ammonia was negligible or the current rapidly dropped towards zero (Figure 1F), the material being tested was considered to be likely inactive towards the AOR. For averaged chronoamperograms of all materials tested, including control experiments showing the lack of any measurable AOR activity of the unmodified carbon fibre paper electrodes, see Section 4 of the Supporting Information.

Immediately prior to and following chronoamperometric measurements where ammonia was present, small samples were collected from the electrolyte solution for product analysis by ion chromatography (Figure 1G–I). The peak that follows NO_2^- at ca. 5.7 min was found to be in good agreement with that of the cyanate anion $[O{=}C{=}N]^-$ (Figure S3 in the Supporting Information). It was present in all ion chromatograms obtained in this work and was shown to be due to the electrooxidation of the carbon fibre paper (CFP) support under the conditions tested herein. Adventitious carbonate was also expectedly detected in all samples (exemplified in Figure S3).

The relative yields of NO_2^- and NO_3^- were used to classify the materials as having "high", "medium", or "low" AOR activity towards $NO_{2/3}^-$ production under the prescribed test conditions. The combined yield of NO_2^- and NO_3^- was considered for

ultimate judgement of "high", "medium" and "low" performance. The relative contributions of NO_3^- and NO_2^- to the combined yield was also taken into consideration as nitrate is generally considered to be the more desirable of the two. Other major products formed during the electrooxidation experiments are N_2 and O_2, while electrooxidation of the electrode itself contributed minimally to the measured currents. Indeed, the average charge passed in the control experiments with unmodified electrodes (metal free) was 0.20 ± 0.07 C and the maximal theoretical amount of charge required to oxidise the deposited metal-based particles (assuming complete transformation of a pure metallic into the highest possible oxidation state) is not higher than 0.07 C (for Mn), which corresponds to not more than ca. 3% of the overall charge passed for the catalytically active systems examined. As there was no pre-existing directly comparable standard to measure against, particularly when catalyst loading and reaction conditions are considered, an internal standard was needed. As such, it was decided that the highest performing catalyst would be treated as a standard against which other materials are measured.

The highest performer in terms of the $NO_{2/3}^-$ production rates were the nickel-based electrodes (Table 1). Thus, our high, medium and low classifications are based on a percentage of the average product yield achieved with Ni and are quoted as percent nickel equivalent (% Ni_{eq}). Catalysts that generated 30% Ni_{eq} or higher for NO_2^- or NO_3^- were considered as having high levels of production. Catalysts that produced between 10% and 30% Ni_{eq} were ranked as having medium production levels, while those falling below 10% Ni_{eq} were classified as having low production levels. Examples of ion chromatograms corresponding to these ratings are shown in Figure 1G–I and the corresponding relative yield data are listed in Table 1. For

ChemSusChem

Research Article
doi.org/10.1002/cssc.202200614

Chemistry
Europe
European Chemical
Societies Publishing

Table 1. Performance of the surveyed catalysts for $NO_{2/3}^-$ synthesis during the AOR.[a]

Catalyst	Faradaic efficiency [%]		Yield [μmol]		$[NO_n^-/\text{total }NO_{2/3}^-]$ [%][b]		Relative yield [% Ni$_{eq}$]	
	NO_2^-	NO_3^-	NO_2^-	NO_3^-	NO_2^-	NO_3^-	NO_2^-	NO_3^-
Ag	0.57±0.06	1.37±0.06	0.048±0.004	0.088±0.008	35±2	65±2	4.3±0.4	4.7±0.4
Bi	0.3±0.3	4.3±1.3	0.005±0.004	0.05±0.01	10±9	90±9	0.4±0.4	2.4±0.6
Ce	0.7±1.2	2±3	0.009±0.02	0.02±0.02	20±40	80±40	1±1	1.1±0.9
Co	0.7±1.2	17±3	0.007±0.012	0.16±0.06	5±9	95±9	1±1	8±3
Cr	0.2±0.1	2±2	0.003±0.001	0.02±0.02	40±50	60±50	0.30±0.05	1.2±1.2
Cu	0±0	18±5	0±0	0.6±0.2	0±0	100±0	0±0	33±13
Fe	0.5±0.4	5.8±0.1	0.02±0.02	0.22±0.03	9±8	91±8	2±2	12±2
Mn	0.5±0.8	4.3±0.9	0.006±0.011	0.05±0.02	10±20	90±20	0.6±1.0	2.5±0.8
Mo	0.3±0.5	3±3	0.001±0.002	0.015±0.004	5±9	95±9	0.1±0.2	0.8±0.2
Nb	7±6	1±2	0.07±0.07	0.02±0.02	60±50	40±50	6±6	1±0.9
Ni	8±2	19±7	1.12±0.10	1.9±0.5	38±8	62±8	100	100
Pb	0±0	3±2	0±0	0.024±0.010	0±0	100±0	0±0	1.3±0.5
Pt	0.3±0.2	5.4±0.9	0.007±0.004	0.08±0.02	8±4	92±4	0.6±0.4	4.0±1.3
Sb	0.3±0.5	0.3±0.5	0.001±0.002	0.005±0.005	30±60	70±60	0.1±0.2	0.3±0.3
Sn	0±0	2.3±0.4	0±0	0.033±0.013	0±0	100±0	0±0	1.7±0.7
Ti	0.1±0.2	3±4	0.001±0.001	0.03±0.02	4±4	96±4	0.09±0.09	1.3±1.3
V	0.3±0.6	2.5±1.0	0.01±0.01	0.03±0.02	20±30	90±30	0.5±0.9	1.5±0.8
Zn	0±0	1±2	0±0	0.02±0.02	0±0	100±0	0±0	1.2±1.2
Zr	3±6	4±2	0.03±0.05	0.03±0.02	30±50	70±50	3±5	1.3±0.9
Control	0.1±0.3	0.2±0.5	0.001±0.002	0.004±0.005	30±60	70±60	0.1±0.2	0.3±0.3

[a] Data were derived from 10 min chronoamperometric tests at 2.000±0.003 V vs. RHE in 0.1 M KOH + 0.1 M NH$_3$ for $n=3$ independent samples of 1 cm^2 electrodes modified with 0.1 μmol cm^{-2} metal and are presented as mean ± standard deviation; relative yield/% Ni$_{eq}$ data show the $NO_{2/3}^-$ yield values normalised to those obtained for the Ni-based electrodes. Control measurements were conducted on equivalent CFP electrodes with no metals deposited on the surface. Catalysts of special interest herein are highlighted with grey shading. [b] Relative contributions of NO_3^- and NO_2^- to the combined $NO_{2/3}^-$ yield.

averaged ion chromatograms of each material tested refer to Section 4 of the Supporting Information.

It should be noted that due to the electrode poisoning issue, which is known to be common in the AOR under ambient conditions, it was decided that quoting yield-rates as is commonly done when describing productivity would not be an appropriate representation of performance as it implies continued operation. As such, for the purposes of this survey, $NO_{2/3}^-$ yields will be generally quoted directly as total μmoles produced in the 10 min chronoamperometric experiments.

From the heatmap of results presented in Figure 1J and the data in Table 1, several metals of interest stand out. Clear indications of activity can be seen in the cyclic voltammograms for cerium, chromium and of course platinum, while cobalt, lead, zinc and zirconium show indications of activity in both voltammetric and chronoamperometric regimes (Section 4 of the Supporting Information). However, all of these materials produced low amounts of $NO_{2/3}^-$, which may indicate that they catalyse conversion of NH$_3$ to N$_2$ (or other non-ionic N-containing products) and as such might be of interest for further studies in this context. However, as the focus of the present work is on the $NO_{2/3}^-$ products, nickel, copper, iron and silver were identified of the highest interest herein. While Ni- and Cu-based electrodes were previously identified as being AOR-active,[25,36] this is not the case for silver and iron. Below, the AOR performance of the electrodes functionalised with these 4 metals is discussed in further detail.

Nickel

While nickel-based electrodes did not score high in all of the tested categories, they were by far the most productive and therefore considered to be the best electrocatalysts for the ammonia to nitrate/nitrite oxidation under the conditions tested herein. Interestingly, despite the activity of Ni/CFP towards the AOR being clearly evident in the product yield, these electrodes produced only moderate changes in cyclic voltammetry and chronoamperometric curves when ammonia was added to the electrolyte solution (Figure 2A,B).

While there are clear changes in the precatalytic region of the voltammetric curves (Figure 2A), the oxidative wave at potentials more positive than ca. 1.7 V vs. RHE was nearly unaffected by the addition of ammonia. This feature is also reflected in chronoamperometry, with the oxidative current densities recorded in the presence of NH$_3$ being only slightly higher in magnitude than those obtained with the ammonia-free solutions (Figure 2B). Given that OH$^-$ is the primary reactant in the OER under alkaline conditions, and NH$_3$ was present at the same concentration (0.1 M) in all experiments discussed herein, we would expect a significant degree of competition between the ammonia oxidation and oxygen evolution processes.[41] Indeed, the average faradaic efficiency (FE) of the nickel-catalysed AOR was 8±2% for NO$_2^-$ and 19±7% for NO$_3^-$, giving a total of 27±9% FE for $NO_{2/3}^-$. Moreover, there were likely contributions from the electrooxidation of ammonia to N$_2$ and hydroxylamine,[42] which were not quantified herein as these products were not the focus of the present study. As such, we are left with the conclusion that the AOR to $NO_{2/3}^-$ is reasonably effective on nickel-based electrodes under

ChemSusChem

Research Article
doi.org/10.1002/cssc.202200614

**Chemistry
Europe**
European Chemical
Societies Publishing
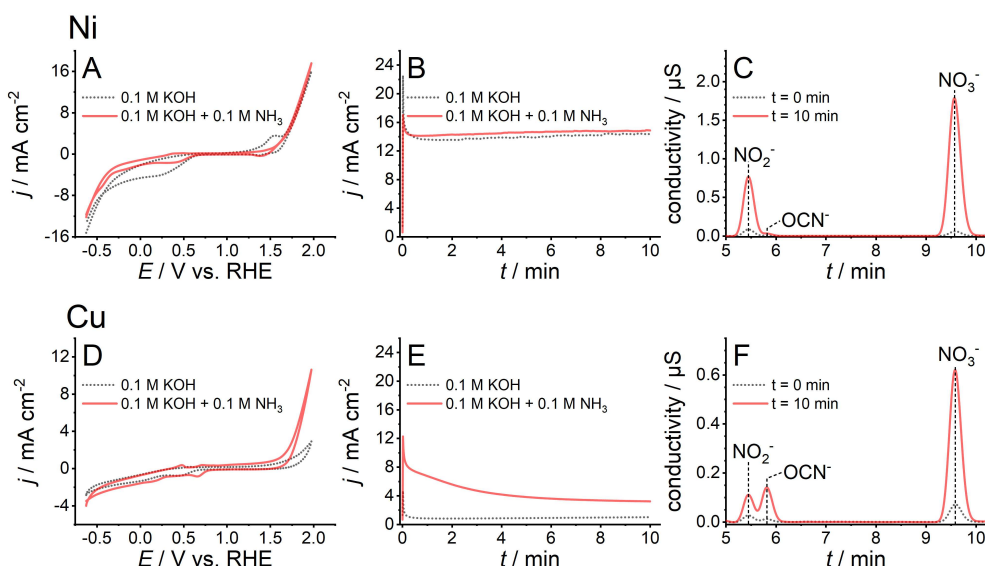
Figure 2. AOR to nitrite/nitrate performance of (A–C) Ni and (D–F) Cu immobilised on CFP electrodes (initial loading 0.1 μmol cm^{-2}). Averaged (A, D) cyclic voltammograms ($v = 0.100$ V s^{-1}; 2nd cycles), and (B, E) chronoamperograms ($E = 2.000 \pm 0.003$ V vs. RHE) for $n = 3$ independent electrodes recorded in 0.1 M KOH without (dotted black) and with (solid red) 0.1 M NH$_3$ present. (C, F) Averaged ($n = 3$) ion chromatograms of the electrolyte solutions prior to (dotted black) and immediately following (solid red) chronoamperometric tests shown in panels (B, E). Currents are normalised to the geometric surface area of the electrodes (1 cm^2).

the conditions employed, thus there should be ample room for optimisation, for example, through modifications such as those reported in the work from Shih et al.[25,43] or Medvedev et al.[37]

Copper

Of the 19 metals tested, copper was the only one to attain a high rating in all of the criteria considered. In cyclic voltammograms, there is a clear and persistent increase in the oxidative current at potentials corresponding to the onset of the Cu^{3+} formation, just prior to the onset of the OER (Figure 2D), as established and discussed in detail in our previous work.[36] This is reflected in chronoamperometry with a major increase in the oxidative current in the presence of ammonia (Figure 2E). Copper-based electrodes are less active for the OER than the Ni-based electrodes, thus the sharp increase in the oxidation rate when the AOR is taking place is expected. However, while there were clear signs of activity for the oxidation of ammonia, Cu was significantly less productive in terms of the product yields. It generated only about one third of the average quantity of NO$_3^-$ produced on nickel-based electrodes (Table 1). At the same time, Cu-based electrodes also proved to be the only catalyst enabling exclusive formation of nitrate rather than nitrite under the chosen test conditions, with a faradaic efficiency just below that of nickel-based electrodes at 18 ± 5%.

As such, copper was concluded to have high levels of activity overall. The high preference for NO$_3^-$ seen here was somewhat unexpected when compared with previous work on Cu metal electrodes where the contribution of NO$_3^-$ to the overall NO$_{2/3}^-$ yield was only ~42% in 0.11 M KOH + 0.1 M

NH$_3$.[36] This apparent inconsistency might be associated with very different morphology and amount of copper on the electrode surface (0.1 μmol cm^{-2} in this work vs. bulk Cu electrodes in Ref. [36]), which would affect the concentration of dissolved Cu species, as well as with the presence of dissolved oxygen in the experiments reported herein in contrast to Ar-saturated solutions used in our previous work.[36] The importance of the latter aspect is discussed later in the text.

Silver

Unlike nickel and copper, the AOR activity of silver-based electrodes is not well documented. Silver has seen use as an alloy with copper in non-electrochemical catalytic ammonia oxidation with the aim of remediating NH$_3$ from waste-water, that is, when N$_2$ is the target product.[44–46] However, in the tests conducted herein, Ag-modified CFP did show clear and consistent signs of activity detected in both voltammetric and chronoamperometric tests (Figure 3A,B). The apparent onset of the AOR was at ca. 1.6 V vs. RHE, which coincides with the reversible oxidation process detected in the absence of ammonia, and most likely associated with the formation of a highly oxidised form of the metal, viz. silver(III)[47] (for reference, the Pourbaix diagram for Ag is set out in Figure S4).

However, both the NO$_{2/3}^-$ product yield and faradaic efficiencies with the silver-based electrodes were relatively low, with only 0.048 ± 0.004 μmol of NO$_2^-$ and 0.088 ± 0.008 μmol of NO$_3^-$ generated on average (Table 1). As this was in stark contrast to the clear signs of ammonia oxidation activity present in electrochemical data, it is likely that alternate
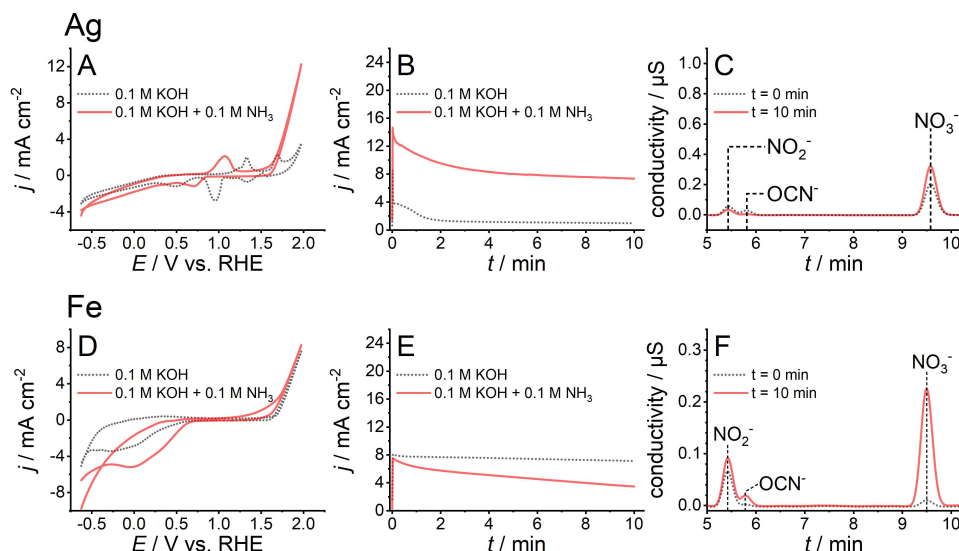
Figure 3. AOR to nitrite/nitrate performance of (A–C) Ag and (D–F) Fe immobilised on CFP electrodes (initial loading 0.1 μmol cm^{-2}). Averaged (A, D) cyclic voltammograms ($v = 0.100$ V s^{-1}; 2nd cycles), and (B, E) chronoamperograms ($E = 2.000 \pm 0.003$ V vs. RHE) for $n = 3$ independent electrodes recorded in 0.1 M KOH without (dotted black) and with (solid red) 0.1 M NH$_3$ present. (C, F) Averaged ($n = 3$) ion chromatograms of the electrolyte solutions prior to (dotted black) and immediately following (solid red) chronoamperometric tests shown in panels (B, E). Currents are normalised to the geometric surface area of the electrodes (1 cm^2).

products are being formed when using Ag/CFP. It was noted that no bubbles were formed during the experiments with silver-based electrodes suggesting that NH$_3$ is oxidised with the formation of soluble compounds, hydroxylamine being one plausible product. Some of the oxidative charge passed might be also associated with the oxidation of the silver itself, promoted by the presence of NH$_3$. Thus, Ag provides an example where very significant oxidation currents are seen in electrochemical measurements, but the product analysis demonstrates low amounts of the target products formed.

It is also important to note that silver oxides are soluble under alkaline conditions[48] and this effect is further promoted by the presence of ammonia[49] rendering the monometallic Ag-based catalyst intrinsically unstable during the AOR. This was observed herein through the SEM analysis of the electrodes before and after chronoamperometric test, which revealed a decrease in the density of Ag-based particles induced by the AOR (Figure S2). With this in mind and considering the capability of this catalyst to promote the initial stages of NH$_3$ oxidation, we hypothesise that silver may prove useful when combined with other catalytic and stabilising oxides. This is a worthy topic of future research.

Iron

Iron has been previously documented as being active for the AOR in dry, pure ammonia systems where the target product was N$_2$.[50] The same study also reported that even trace amounts of water in the system induced rapid electrode poisoning. However, where NO$_{2/3}^-$ are the target compounds, the results tell a different story. In contrast to the silver-based electrodes, Fe/CFP demonstrated modest changes in cyclic voltammetry and chronoamperometric measurements when ammonia was added to the electrolyte solution (Figure 3D,E). Specifically, there was a slight increase in the oxidative current in the anodic voltammetric sweeps between ca. 1.1 and 1.75 V vs. RHE. At more positive potentials, the current rises up to follow the same OER oxidation wave as was seen in the absence of NH$_3$. In a departure from what was seen with nickel-, copper- and silver-based electrodes, currents measured for the iron-functionalised CFP at a constant potential of 2 V vs. RHE dropped in the presence of ammonia, suggesting deactivation of the catalyst (Figure 3E).

With a faradaic efficiency of $6.3 \pm 0.5\%$ for NO$_{2/3}^-$ and a relative yield of $2.0 \pm 1.9\%$ and $11.7 \pm 1.6\%$ Ni$_{eq}$ (0.02 $\pm$ 0.02 and 0.22 $\pm$ 0.03 μmol) for NO$_2^-$ and NO$_3^-$, respectively, iron-based electrodes cannot be considered to be high-performing catalysts for the AOR (Table 1). However, product yields were highly reproducible. As such, this system was deemed worthy of further investigation. Upon completing several longer-term experiments under differing conditions, some unusual behaviour was observed. Specifically, the electrocatalytic performance of the Fe/CFP electrodes was impacted by the presence of dissolved oxygen. This can be seen from comparisons of the NO$_{2/3}^-$ yield data obtained during 1 h chronoamperometric experiments at 2 V vs. RHE in the presence of ammonia in a gastight cell with argon- (Figure 4A) or O$_2$-saturated (Figure 4B) electrolyte solutions. Specifically, a 20-fold increase in the yield of NO$_3^-$ was seen when oxygen was present in the system, with yields of 0.9 and 2.0 μmol for NO$_2^-$ and NO$_3^-$ (total NO$_{2/3}^-$ faradaic efficiency of ~14%), respectively, as opposed to yields of 0.0 and 0.1 μmol (total NO$_{2/3}^-$ faradaic efficiency of ~1%) when saturated with argon. Therefore, it is apparent that
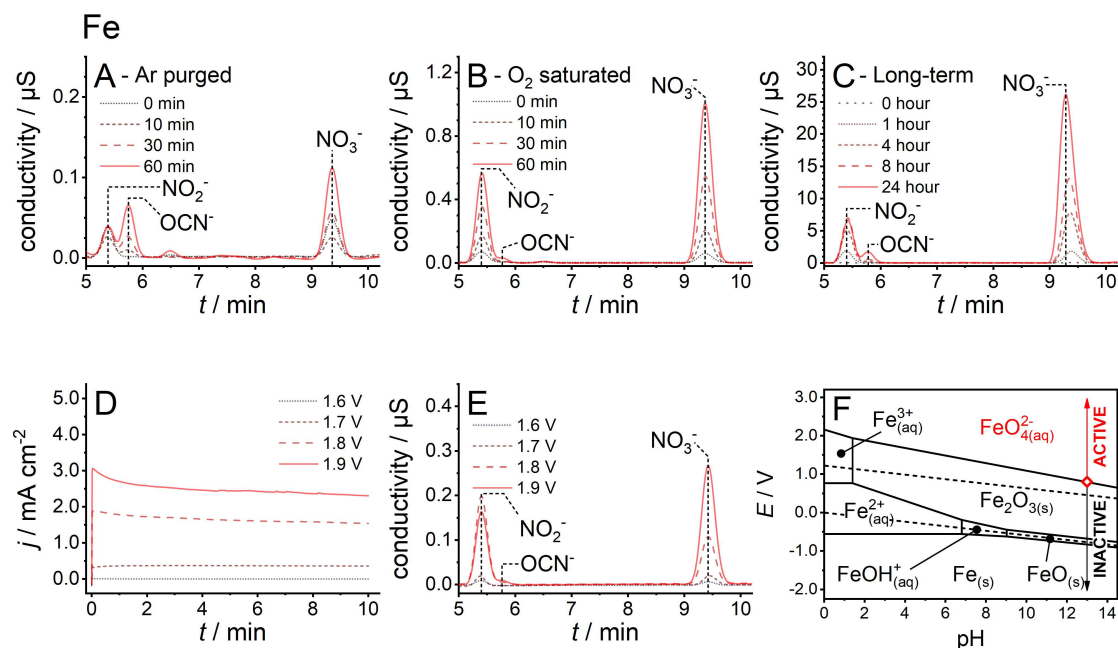
Figure 4. (A–C) Ion chromatograms of the (A) Ar-, (B) O_2- and (C) air-saturated 0.1 M KOH + 0.1 M NH_3 electrolyte solutions collected during chronoamperometric (2.00 V vs. RHE) tests of Fe/CFP under respective atmospheres. (D) Chronoamperograms collected during electrooxidation of air-saturated 0.1 M KOH + 0.1 M NH_3 with Fe/CFP at 1.6 (dotted black), 1.7 (short dashed brown), 1.8 (long dashed dark-red) and 1.9 V vs. RHE (solid red), and (E) corresponding ion chromatograms of the final solutions. (F) Pourbaix diagram of iron ([Fe] = 1×10^{-6} M, 298 K, 1 atm)[51] with the apparent onset potential of the AOR at pH 13 used in the present work marked with a red diamond symbol.

dissolved molecular oxygen is a key reactant in the case of Fe/CFP for the production of $NO_{2/3}^-$.

With the knowledge that oxygen is required to support the reaction, longer-term chronoamperometric testing was undertaken to discern if Fe/CFP electrodes would continue to produce $NO_{2/3}^-$ consistently (Figure S5A). As can be seen in ion chromatograms collected from 24 h of chronoamperometry at 1.9 V vs. RHE, iron-based electrodes were able to continuously produce NO_3^- in a near linear fashion with air-saturated electrolyte solutions (Figure 4C). This process, while relatively stable, was still slow with an average NO_3^- yield of 6–13 μmol after 24 h at a faradaic efficiency of 9–10%. This corresponds to an approximate rate of 0.14–0.18 nmol s^{-1} cm^{-2}, that is, significantly lower than the performance of Ni/CFP measured in short 10 min tests (Table 1). However, the rate of NO_3^- production during the Ni-catalysed AOR in a 24 h measurement was found to be only 0.06–0.08 nmol s^{-1} cm^{-2} at a faradaic efficiency of 1–2% (Figure S5B), meaning that Fe/CFP maintains production rates and efficiency better than Ni/CFP over longer durations. Stable long-term ammonia electrooxidation with high preference for NO_3^- (relative to nickel-based electrodes) is quite uncommon. Therefore, this result identifies iron-based materials as promising AOR catalysts for future study and optimisation.

With the dependence on molecular oxygen established and long-term operation shown to be possible, a brief investigation into the active form of iron was conducted. There was evidence in cyclic voltammetry that the onset potential for the AOR could be as low as ca. 1.1 V vs. RHE (Figure 3D). This was tested by running a series of 10 min chronoamperometric measurements

at 1.9, 1.8, 1.7 and 1.6 V vs. RHE. As can be seen in Figure 4D, there is a significant stepdown in current at 1.7 V relative to 1.8 and 1.9 V, while at 1.6 V vs. RHE the current was negligible. These results are reflected in the $NO_{2/3}^-$ yields, with 1.9 and 1.8 V vs. RHE generating ca. 0.53 and 0.19 μmol, respectively, while 1.7 V vs. RHE generated only 0.03 μmol. There were no products of interest generated at detectable levels at 1.6 V vs. RHE (Figure 4E). Based on this we can predict that the active form of iron for the AOR to $NO_{2/3}^-$ forms between 1.6 and 1.7 V vs. RHE. At pH 13, this potential matches the transition between Fe_2O_3 and FeO_4^{2-} (Figure 4F), which might point to a contribution from a homogeneous redox reaction involving highly oxidised form of iron to the mechanism of the process, similar to Cu as discussed elsewhere.[36]

Conclusion

The goal of this study was to classify a range of metals for their activity towards the electrocatalytic oxidation of NH_3 to form $NO_{2/3}^-$. Of the methods used to screen the AOR activity of the metal-based electrodes tested here, product analysis via ion chromatography was expectedly the most useful to this principal aim of the study. In this regard, nickel-functionalised electrodes were the most active of the materials tested with a rate of 5.0 ± 1.0 nmol s^{-1} cm^{-2}, $62 \pm 8\%$ of which was towards NO_3^- production during short-term 10 min tests. The next most active in terms of productivity were copper-based electrodes, with a yield rate of 1.0 ± 0.4 nmol s^{-1} cm^{-2}, which is however

only about 20% of the performance of the Ni/CFP electrode, albeit with an exclusive formation of the more desirable nitrate product.

Most interestingly, the survey study also identified silver and iron as potentially promising components for catalysts for the NH_3 electrooxidation to nitrite and nitrate. Silver-functionalised electrodes showed strong evidence of the AOR activity in electrochemical experiments but had relatively low rates of $NO_{2/3}^-$ production, suggesting that alternate oxidation products are formed. The propensity of the oxidised forms of silver to dissolve in alkaline ammonia solutions is also an important limiting factor. Nonetheless, Ag could prove useful as a component facilitating the initial steps of NH_3 oxidation stabilised within multimetallic catalysts. Iron-based electrodes on the other hand, showed a strong correlation between the presence of dissolved oxygen and the rate of $NO_{2/3}^-$ production. At low concentrations of O_2, Fe/CFP showed a marked drop in activity, while operation in solutions saturated with oxygen enabled steady performance. Importantly, while product yields from short-term chronoamperometric measurements for the iron-based catalyst were significantly lower than those attained with Ni/CFP, 24 h experiments revealed an opposite trend. Specifically, Fe/CFP electrodes maintained their activity better than Ni/CFP, with an overall yield rate of 0.12 ± 0.02 nmol s^{-1} cm^{-2} and a faradaic efficiency of $10 \pm 2\%$. These results call for extended investigations of the iron-based materials as promising catalysts among non-noble-metal systems, for practical ammonia electrooxidation to nitrite and nitrate.

Experimental Section

Materials

Electrolyte solutions for the electrochemical measurements were prepared using KOH (Merck; $\geq 85\%$, acidimetric), concentrated NH_4OH solution (14.6 M; Ajax Finechem Pty Ltd. analytical reagent grade) and deionised H_2O, which was produced by a Sartorius™ Arium® Comfort II water purification system and had a resistivity of 18.2 MΩ cm at ambient temperature ($23 \pm 2\,°C$). Water of the same quality was used for all operations requiring H_2O. Due to the hygroscopic nature of solid KOH, reagents were stored under vacuum to prevent absorption of water vapour, and concentrations of 0.1 M KOH solutions were confirmed via titration with HCl.

Catalyst precursors used to produce deposition solutions were $AgC_2H_3O_2$ (ReagentPlus®, 99%), $BiCl_3$ (reagent grade, $\geq 98\%$), $(CH_3COO)_2Co \cdot 4H_2O$ ($\geq 98.0\%$), $CrCl_3$ (99%), $Cu(CO_2CH_3)_2$ (98%), $FeCl_2$ (98%), $MnCl_2 \cdot 4H_2O$ (BioUltra, $\geq 99.0\%$), $MoCl_5$ (95%), $NbCl_5$ (99%), $Ni(OCOCH_3)_2 \cdot 4H_2O$ (98%), $PdCl_2$ (ReagentPlus®, 99%), H_2PtCl_6 (ACS reagent, $\geq 37.50\%$ Pt basis), $SbC_2H_3O_2$ (99.99%), $SnCl_2$ (98%), $Ti(OCH_2CH_2CH_3)_4$ (98%), VCl_3 (97%) and $ZnCl_2$ (reagent grade, $\geq 98\%$) purchased from Sigma-Aldrich, and $ZrCl_4$ (99.5%) as well as CeO_2 (99.5%) purchased from Alfa Aesar. All reagents were used as received. Ar/H_2 (95:5 vol.) gas mixture used during synthesis was provided by Air Liquide (UN 1958). In electrochemical experiments where gas purging was required, high purity Ar gas (UN 1006) purchased from BOC was used. In experiments where saturation with O_2 was required, industrial grade O_2 gas (UN 1072) purchased from BOC was used.

For the ion chromatography calibration, $NaNO_2$ (ReagentPlus®, $\geq 99.0\%$), $NaNO_3$ (ACS reagent, $\geq 99.0\%$) and NaOCN (96%) purchased from Sigma-Aldrich were used.

Preparation of electrodes

Carbon fibre paper (CFP) (Spectracarb™ 2050 A-1550; thickness = 0.381 mm) obtained from the Fuel Cell Store was cut into 2 cm × 1 cm segments to serve as catalyst substrates. Prior to use, these electrodes were treated with freshly made 'piranha' solution (a 3:1 vol. mixture of reagent grade concentrated H_2SO_4 from Ajax Finechem and analytical grade 30 wt% H_2O_2 from EMSURE®) for 12 h. This process was used to enhance the hydrophilicity of the CFP surface, resulting in improved contact between the electrode and the deposition solution. Following this treatment, electrodes were washed via repeated cycles of sonication (Branson B5500R-dth bath with an operating power of 175 W) and rinsing with water and then placed in a covered glass dish and allowed to dry in a small benchtop oven at 80 °C over ca. 16 h. Deposition solutions were produced in a 2-step process. First, a mass of the desired metal salt equating to the amount needed to produce a 10 mM solution was fully or partially dissolved in glacial acetic acid. Following this, initial solutions were diluted by a factor of 10 in isopropanol, effectively dissolving any remaining solid material to form a 1 mM solution. Each CFP electrode was modified by drop-casting a total of 100 µL of the precursor solution in 10 µL aliquots (5 applications per side over the 1 cm^2 area of the electrode to be submerged during electrochemical measurements), with sufficient time in between aliquots for the solvent to evaporate giving an approximate loading of 0.1 µmol cm^{-2}. Following drop-casting, electrodes were annealed under an Ar/H_2 (95:5 vol.) flow (~ 10 mL min^{-1}) in a quartz tube furnace. The temperature was adjusted in a pre-programed pattern, first being held at 100 °C for 1 h to ensure that electrodes were dry, then raised to 550 °C at a ramp-rate of 5 °C per minute and held at that temperature for another 3 h to facilitate catalyst reduction. Upon completion, the gas was switched to pure Ar at a flow rate of ~ 10 mL min^{-1} and the system was allowed to cool to room temperature naturally before electrodes were exposed to air. All electrodes were rinsed with water and used within 72 h after preparation.

Electrochemical measurements

All electrochemical measurements were conducted using Gamry Instruments Interface 1000-E potentiostats in a standard three-electrode configuration. Experiments were typically conducted in a set of glass "H-cells" with the two compartments separated by a low-porosity P4 (10–16 µm pore size) ceramic frit with an electrolyte solution volume of 10 mL per compartment. Experiments under controlled atmosphere were conducted in a dual compartment Teflon cell divided by a Nafion 115 membrane (thickness = 127 µm) purchased from the Fuel Cell Store. The headspace of both compartments was connected via a bridge of nylon tubing (1 mm internal diameter) to equalise the gas pressure and prevent electrolyte flow between compartments. Water locks were placed inline at both the inlet and outlet of the cell to prevent the backflow of atmosphere into the headspace. Gas (Ar or O_2) was flowed through the cell at a rate of ~ 30 mL min^{-1}. Both oxygen and argon gas were bubbled through a saturator filled with H_2O prior to entering the cell. Electrolyte solution volume was 10 mL in the working electrode compartment and ~ 4 mL in the auxiliary electrode compartment.

Each experiment was conducted with an initial 0.1 M KOH electrolyte solution where NH_4OH (14.6 M) was subsequently added into the electrolyte solution in a 70 µL aliquot following preliminary

ChemSusChem

Research Article
doi.org/10.1002/cssc.202200614

**Chemistry
Europe**
European Chemical
Societies Publishing

measurements in the absence of ammonia for a total starting concentration of 0.1 M NH_3. Electrolyte solution samples of 0.1 mL were extracted for analysis prior to the commencement of chronoamperometry in the presence of NH_3, and immediately after the measurement was concluded. In order to avoid any catalytic contributions from the electrode connector, CFP electrodes were mounted in small rigid titanium mesh envelopes, which were held clear of the electrolyte solution during testing. Only the modified part of the electrode (ca 1 cm²) was immersed in the electrolyte solution during experiments.

The auxiliary electrode was a platinised titanium mesh plate. Due to the pervasive nature of ammonia, a custom-designed reference system[36] was employed to ensure that electrode potentials remained stable throughout the course of testing. This was achieved via the use of a narrow, agar-filled PTFE tube which served as a salt bridge, connecting the electrolyte solution to a standard Ag | AgCl | KCl$_{sat.}$ (CHI instruments) reference electrode (Section 8 of the Supporting Information). The design proved effective, with an average potential of 0.198 ± 0.003 V vs. standard hydrogen electrode (SHE) at an average temperature 23 ± 2°C which was calculated via regular measurements against a saturated calomel master reference electrode. Reference electrode potentials were habitually measured and recorded prior to use to ensure accurate conversion potentials for the measurements that followed. Measured potentials were converted to the reversible hydrogen electrode (RHE) scale using the Nernst equation and pH values determined by titration. Unless explicitly stated otherwise, all potential values specified herein are quoted relative to the RHE scale.

Ion chromatography

Concentrations of $NO_{2/3}^-$ in the electrolyte solutions were quantified by ion chromatography (IC) on a DIONEX Integrion high pressure ion chromatograph from ThermoFisher Scientific equipped with an ionic conductivity detector, a Dionex ADRS 600 2 mm RFIC Electrolytically regenerated conductivity suppressor and a Dionex IonPac AS1-HC-4 μm high-capacity analytical column/Dionex IonPac AG11-HC-4 μm high-capacity guard column combination (2 mm column diameter). Analysis of chromatograms was done using the Chromeleon 7.2.10 ES ThermoFisher Scientific software suite.

Sample preparation was done by diluting the electrolyte solution samples (0.1 mL) by a factor of 10 with water to achieve a similar KOH concentration and pH as in the IC eluent. pH adjustment with an acid was impractical in this case as the conjugate base competes with the analytes for interaction with the solid phase of the column.

Each individual measurement consisted of a 20 min run at a flow rate of 0.380 mL min⁻¹. A custom eluent gradient was developed for the task of quantifying both NO_2^- and NO_3^- in 0.1 M KOH + 0.1 M NH_3 solutions, as well as providing adequate separation of other anions present in solutions, viz. carbonate and cyanate (Figure S6). In this gradient, the KOH eluent concentration is kept constant at 8 mM from 0 to 11 min, then sharply increased to 40 mM at a ramp rate of 20 mM min⁻¹. The ramp is then reversed at the same rate, returning to a value of 8 mM at the 15 min mark, continuing through at that level until the measurement is concluded at the 20 min mark (Figure S6). All key components, including the conductivity detection cell, conductivity suppressor, column and eluent lines were maintained at a temperature of 30°C during measurements.

Scanning electron microscopy

SEM characterisation was conducted on a FEI Quanta 3D FIBSEM at an accelerating voltage of 15 kV (data shown in Figure S1) and a JEOL JSM-7001F FEG-SEM at an accelerating voltage (HT) of 15 kV (data shown in Figure S2). The samples were attached to the SEM specimen holders or supporting stubs by a double-sided conducting carbon tape. No additional coatings were applied to the SEM samples.

X-ray diffraction

XRD patterns were recorded using a Bruker D8 Advance X-ray diffractometer with Cu K$_\alpha$ radiation source (40 mA and 40 kV) within a 2θ range of 30°–80° with a 0.02° step and 0.5 s step⁻¹. Electrodes were attached to a flat, low background powder specimen holder and analysed directly.

X-ray photoelectron spectroscopy

XPS data were collected using a Thermo Scientific Nexsa Surface Analysis System equipped with a hemispherical analyser under pressure between 10^{-9} and 10^{-8} mbar using monochromatic Al K$_\alpha$ X-ray beam (1486.6 eV) at 72 W (12 kV × 6 mA) at an incident angle of 45°. A low-energy dual-beam (ion and electron) flood source was used for charge neutralisation. The X-ray spot size was 400 μm × 800 μm. For survey scans, the pass energy, voltage step size and dwell time were 200 eV, 1 eV and 10 ms, respectively. For the high-resolution scans, these parameters were 50 eV, 0.1 eV and 50 ms, respectively, typically yielding a full width at half maximum (FWHM) value of 0.86–0.87 eV for the Ag 3d$_{5/2}$ peak and < 1.0 eV for the main C 1s peak in PET during performance tests.

The samples were analysed at a nominal photoelectron emission angle of 0° with respect to the surface normal. Since the actual emission angle is ill-defined in the case of rough surfaces as in the present case (ranging from 0° to 90°) the sampling depth may range from 0 to approximately 10 nm. Data processing was performed using Avantage software version 5.9902. All elements presented were identified from survey spectra. All binding energies were charge corrected to the adventitious C 1s peak at 284.8 eV. At least two different spots on each sample were probed to ensure the consistency of the results.

Conflict of Interest

D.R.M. and A.N.S. have minority equity ownership, as well as management and consulting roles, in Jupiter Ionics Pty Ltd.

Data Availability Statement

The data that support the findings of this study are available from the corresponding author upon reasonable request.

[1] T. Wilhelm, A. Biltz, *Ber. Dtsch. Chem. Ges.* **1904**, *37*, 3130–3138.
[2] B. A. López De Mishima, D. Lescano, T. Molina Holgado, H. T. Mishima, B. A. L. De Mishima, D. Lescano, T. M. Holgado, H. T. Mishima, *Electrochim. Acta* **1998**, *43*, 395–404.
[3] A. Galdikas, A. Mironas, V. Strazdien, A. S̃etkus, I. Ancutien, V. Janickis, *Sens. Actuators B.* **2000**, *67*, 76–83.
[4] X. Ji, C. E. Banks, R. G. Compton, *Analyst* **2005**, *130*, 1345–1347.
[5] L. Marinčić, F. B. Leitz, *J. Appl. Electrochem.* **1978**, *8*, 333–345.
[6] E. P. Bonnin, E. J. Biddinger, G. G. Botte, *J. Power Sources* **2008**, *182*, 284–290.
[7] L. Li, Y. Liu, *J. Hazard. Mater.* **2009**, *161*, 1010–1016.
[8] H. Zöllig, C. Fritzsche, E. Morgenroth, K. M. Udert, *Water Res.* **2015**, *69*, 284–294.
[9] L. A. Diaz, G. G. Botte, *Electrochim. Acta* **2015**, *179*, 529–537.
[10] F. Vitse, M. Cooper, G. G. Botte, *J. Power Sources* **2005**, *142*, 18–26.
[11] S. Giddey, S. P. S. Badwal, C. Munnings, M. Dolan, *ACS Sustainable Chem. Eng.* **2017**, *5*, 10231–10239.
[12] E. J. Cairns, E. L. Simons, A. D. Tevebaugh, *Nature* **1968**, *217*, 780–781.
[13] E. L. Simons, D. J. Surd, E. J. Cairns, *J. Electrochem. Soc.* **1969**, *116*, 131–138.
[14] S. Suzuki, H. Muroyama, T. Matsui, K. Eguchi, *J. Power Sources* **2012**, *208*, 257–262.
[15] M. H. M. T. Assumpção, S. G. Da Silva, R. F. B. De Souza, G. S. Buzzo, E. V. Spinacé, A. O. Neto, J. C. M. Silva, *Int. J. Hydrogen Energy* **2014**, *39*, 5148–5152.
[16] J. Zawadzki, *Discuss. Faraday Soc.* **1950**, *8*, 140–152.
[17] T. Katan, R. J. Galiotto, *J. Electrochem. Soc.* **1963**, *110*, 1022.
[18] H. G. Oswin, M. Salomon, *Can. J. Chem.* **1963**, *41*, 1686–1694.
[19] H. Gerischer, A. Mauerer, *J. Electroanal. Chem.* **1970**, *25*, 421–433.
[20] N. M. Adli, H. Zhang, S. Mukherjee, G. Wu, *J. Electrochem. Soc.* **2018**, *165*, J3130–J3147.
[21] Z. F. Li, Y. Wang, G. G. Botte, *Electrochim. Acta* **2017**, *228*, 351–360.
[22] K. Siddharth, Y. Chan, L. Wang, M. Shao, *Curr. Opin. Electrochem.* **2018**, *9*, 151–157.
[23] A. Kapałka, A. Cally, S. Neodo, C. Comninellis, M. Wächter, K. M. Udert, *Electrochem. Commun.* **2010**, *12*, 18–21.
[24] L. Candido, J. A. C. P. Gomes, *Mater. Chem. Phys.* **2011**, *129*, 1146–1151.
[25] Y. J. Shih, Y. H. Huang, C. P. Huang, *Electrochim. Acta* **2018**, *263*, 261–271.
[26] A. C. A. de Vooys, M. T. M. Koper, R. A. Van Santen, J. A. R. Van Veen, *J. Electroanal. Chem.* **2001**, *506*, 127–137.
[27] P. N. Cheremisinoff, in *Waste Minimization Cost Reduct. Process Ind.*, Elsevier, **1995**, pp. 222–284.
[28] Z. Kirova-Yordanova, *Energy* **2011**, *36*, 3733–3744.
[29] V. Smill, R. A. Streatfeild, *Enriching the Earth: Fritz Haber, Carl Bosch, and the Transformation of World Food Production*, MIT Press, **2002**.
[30] D. Reay, C. Sabine, P. Smith, G. Hymus, *Intergovernmental Panel on Climate Change. Fourth Assessment Report. Geneva, Switzerland: Inter-Gov- Ernmental Panel on Climate Change. Cambridge; UK: Cambridge University Press; 2007. Available from: www.Ipcc.Ch.*, Intergovernmental Panel On Climate Change, **2007**.
[31] W. Laue, M. Thiemann, E. Scheibler, K. W. Wiegand, in *Ullmann's Encycl. Ind. Chem.*, Wiley-VCH Verlag GmbH & Co. KGaA, Weinheim, Germany, **2000**.
[32] A. P. Akolzin, Y. Y. Kharitonov, S. G. Kovalenko, *Mater. Corros.* **1987**, *38*, 417–421.
[33] F. Almomani, R. Bhosale, M. Khraisheh, A. Kumar, M. Tawalbeh, *Int. J. Hydrogen Energy* **2020**, *45*, 10398–10408.
[34] M.-H. Tsai, T.-C. Chen, Y. Juang, L.-C. Hua, C. Huang, *Electrochem. Commun.* **2020**, *121*, 106875.
[35] W. Xu, R. Lan, D. Du, J. Humphreys, M. Walker, Z. Wu, H. Wang, S. Tao, *Appl. Catal. B* **2017**, *218*, 470–479.
[36] S. Johnston, L. Kemp, B. Turay, A. N. Simonov, B. H. R. Suryanto, D. R. MacFarlane, *ChemSusChem* **2021**, *14*, 4793–4801.
[37] J. J. Medvedev, Y. Tobolovskaya, X. V. Medvedeva, S. W. Tatarchuk, F. Li, A. Klinkova, *Green Chem.* **2022**, *4*, 1578–1589.
[38] M. S. Burke, S. Zou, L. J. Enman, J. E. Kellon, C. A. Gabor, E. Pledger, S. W. Boettcher, *J. Phys. Chem. Lett.* **2015**, *6*, 3737–3742.
[39] M. S. Burke, L. J. Enman, A. S. Batchellor, S. Zou, S. W. Boettcher, *Chem. Mater.* **2015**, *27*, 7549–7558.
[40] J. F. E. Gootzen, A. H. Wonders, W. Visscher, R. A. van Santen, J. A. R. van Veen, *Electrochim. Acta* **1998**, *43*, 1851–1861.
[41] G. Li, L. Anderson, Y. Chen, M. Pan, P.-Y. Abel Chuang, *Sustain. Energy Fuels* **2018**, *2*, 237–251.
[42] K. Sasaki, Y. Hisatomi, *J. Electrochem. Soc.* **1970**, *117*, 758.
[43] Y. J. Shih, Y. H. Huang, C. P. Huang, *Electrochim. Acta* **2018**, *281*, 410–419.
[44] L. Gang, B. G. Anderson, J. Van Grondelle, R. A. Van Santen, W. J. H. Van Gennip, J. W. Niemantsverdriet, P. J. Kooyman, A. Knoester, H. H. Brongersma, *J. Catal.* **2002**, *206*, 60–70.
[45] M. Yang, C. Wu, C. Zhang, H. He, *Catal. Today* **2004**, *90*, 263–267.
[46] M. Jabłońska, A. M. Beale, M. Nocuń, R. Palkovits, *Appl. Catal. B* **2018**, *232*, 275–287.
[47] F. Pargar, D. Koleva, *Int. J. Struct. Civ. Eng. Res.* **2017**, 172–176.
[48] R. F. Amlie, P. Rüetschi, *J. Electrochem. Soc.* **1961**, *108*, 813.
[49] B. Tollens, *Ber. Dtsch. Chem. Ges.* **1882**, *15*, 1635–1639.
[50] D. J. Little, D. O. Edwards, M. R. Smith, T. W. Hamann, *ACS Appl. Mater. Interfaces* **2017**, *9*, 16228–16235.
[51] K. A. Persson, B. Waldwick, P. Lazic, G. Ceder, *Phys. Rev. B* **2012**, *85*, 235438.